Irradiation Effects of High-Energy Proton Beams on MoS_2 Field Effect Transistors

Tae-Young Kim,[†] Kyungjune Cho,[†] Woanseo Park,[†] Juhun Park,[†] Younggul Song,[†] Seunghun Hong,[†,‡] Woong-Ki Hong,[§] and Takhee Lee[†,*]

[†]Department of Physics and Astronomy and Institute of Applied Physics, Seoul National University, Seoul 151-747, Korea, [‡]Department of Biophysics and Chemical Biology, Seoul National University, Seoul 151-747, Korea, and [§]Jeonju Center, Korea Basic Science Institute, Jeonju, Jeollabuk-do 561-180, Korea

ABSTRACT We investigated the effect of irradiation on molybdenum disulfide (MoS_2) field effect transistors with 10 MeV high-energy proton beams. The electrical characteristics of the devices were measured before and after proton irradiation with fluence conditions of 10^{12}, 10^{13}, and 10^{14} cm^{-2}. For a low proton beam fluence condition of 10^{12} cm^{-2}, the electrical properties of the devices were nearly unchanged in response to proton irradiation. In contrast, for proton beam fluence conditions of 10^{13} or 10^{14} cm^{-2}, the current level and conductance of the devices significantly decreased following proton irradiation. The electrical changes originated from proton-irradiation-induced traps, including positive oxide-charge traps in the SiO_2 layer and trap states at the interface between the MoS_2 channel and the SiO_2 layer. Our study will enhance the understanding of the influence of high-energy particles on MoS_2-based nanoelectronic devices.

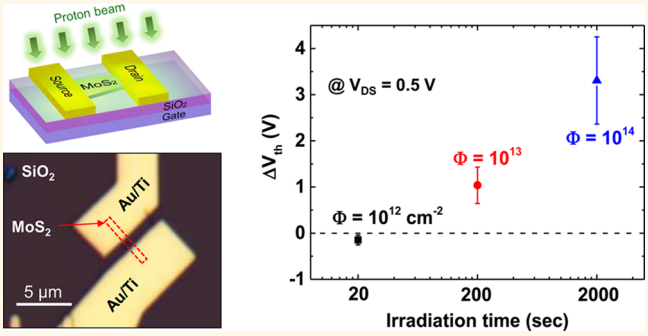

KEYWORDS: molybdenum disulfide (MoS_2) · field effect transistors · proton beam · electronic transport properties

Recently, two-dimensional (2D) transition-metal dichalcogenide (TMD) materials have gained significant attention due to their potential applications in atomic-film devices.[1−4] Graphene, one of the most popular of these 2D materials, has been widely studied but has limited utility as a semiconductor because it lacks an energy band gap.[5] Unlike graphene, TMD materials such as MoS_2, $MoSe_2$, and WSe_2 possess a band gap and semiconducting properties.[6−8] In particular, molybdenum disulfide (MoS_2) has an indirect band gap of 1.2 eV as a bulk material and a direct band gap of 1.8 eV as a single layer.[4,8] Numerous studies have explored the application of 2D TMD materials in nanoelectronic devices because of their semiconducting properties.[9−14] For example, researchers have demonstrated that MoS_2-based field effect transistor (FET) devices have outstanding electrical characteristics; a single-layer MoS_2 device exhibits a high mobility (~200 $cm^2/(V\ s)$) with a near-ideal subthreshold swing down to 74 mV/decade and a high on/off ratio (~10^8).[15]

The ability to tailor the electrical properties of MoS_2 FETs would provide numerous advantages. In particular, to prepare a logic circuit using MoS_2, it is necessary to control the operation voltage. When trap states are introduced at the MoS_2 active layer and dielectric layer, the electrical properties of the device, such as the current and threshold voltage, are affected by charge trapping to these trap states. Attempts to tailor the electrical properties of FET devices made with carbon nanotubes[16,17] or semiconducting nanowires[18−20] have been made using irradiation with high-energy particles. Originally, high-energy particle beams of protons, electrons, or ions were used to impact silicon-based metal-oxide-semiconductor (MOS) devices in order to modify the electrical properties of the devices or investigate the properties under outer space conditions.[21−24]

A few theoretical and experimental studies have investigated the irradiation of MoS_2 materials with electrons, protons, or heavy ions. Komsa *et al.* studied the effects of electron beam irradiation on 2D

* Address correspondence to tlee@snu.ac.kr.

Received for review December 18, 2013 and accepted February 23, 2014.

Published online February 24, 2014
10.1021/nn4064924

TMD materials using first-principle simulations and experimental studies of single-layer MoS_2 devices irradiated by electron beams in a transmission electron microscope (TEM) operating at 20 keV.[25] Ochedowski *et al.* demonstrated the deterioration of MoS_2 FETs following 1.14 GeV U^{28+} ion beam irradiation,[26] and Mathew *et al.* studied ferromagnetism in MoS_2 bulk materials following 2 MeV proton beam irradiation.[27] However, a comprehensive study of high-energy particle beams on MoS_2 atomic film-based FET devices has not yet been investigated. Therefore, it would be important to understand and develop irradiation-mediated engineering in MoS_2 FET devices.

Here, we studied the effect of proton irradiation on MoS_2 FET devices prepared with a few layers of MoS_2 flakes. The devices were irradiated with 10 MeV proton beams under fluence conditions of 10^{12}, 10^{13}, and 10^{14} cm^{-2}, corresponding to beam irradiation times of 20, 200, and 2000 s, respectively. We systematically measured and compared the electrical properties of the devices, including current level, conductance, and threshold voltage, before and after proton irradiation for each proton beam fluence condition. The changes in the electrical properties of the proton-irradiated devices can be attributed to irradiation-induced traps, such as positive oxide-charge traps in the SiO_2 layer and interface trap states.

RESULTS AND DISCUSSION

We fabricated MoS_2 FET devices using the following process. First, we transferred MoS_2 flakes from a bulk MoS_2 crystal (purchased from SPI Supplies, USA) onto Si wafer pieces using a mechanical exfoliation method. The Si substrate used in this study had a 270-nm-thick SiO_2 layer on highly doped Si and could be used as a gate electrode. Following the mechanical transfer of the MoS_2 flakes, suitable MoS_2 flakes were located with an optical microscope (Figure 1a). Although it was possible to transfer single-layer MoS_2 films, we more routinely transferred multilayer MoS_2 films comprising a few MoS_2 atomic layers. The thickness of the typically selected MoS_2 flakes was approximately 2−8 nm, as determined by atomic force microscopy (AFM) (Park Systems, NX10) (Figure 1c). Because the thickness of a single MoS_2 layer is 0.65 nm, this flake thickness corresponds to 3−12 layers. After the locations and coordinates of the MoS_2 flake were determined with an electron-beam lithography system, source and drain electrodes were made by depositing Au (100 nm)/Ti (10 nm) with an electron beam evaporator. More detailed information describing the device fabrication is provided in Figure S1 of the Supporting Information.

Following the fabrication of the MoS_2 FET devices, their electrical characteristics were measured. The devices were subsequently irradiated by a proton beam. The proton beam facility used for this research was the MC-50 cyclotron at the Korea Institute of Radiological and Medical Sciences. The proton beam exhibited an energy of 10 MeV, an average beam current of 10 nA, and a beam uniformity of approximately 90%. Beam irradiation times of 20, 200, and 2000 s were investigated, corresponding to total fluence (or dose) values, Φ, of $\sim 10^{12}$, 10^{13}, and 10^{14} cm^{-2}. The fabricated MoS_2 FET devices were divided into three groups according to the proton beam fluence conditions. The electrical characteristics of each device were measured before and after proton irradiation and systematically compared.

Figure 2 illustrates the electrical characteristics of the MoS_2 FET devices. The left and right plots in Figure 2a show the output characteristics (source−drain current *versus* source−drain voltage, $I_{DS}-V_{DS}$) measured for a MoS_2 FET at gate voltages (V_G) ranging from −30 to 30 V in increments of 10 V before and after, respectively, proton beam irradiation with a fluence of 10^{12} cm^{-2} (corresponding to an irradiation time of 20 s). Figure 2b

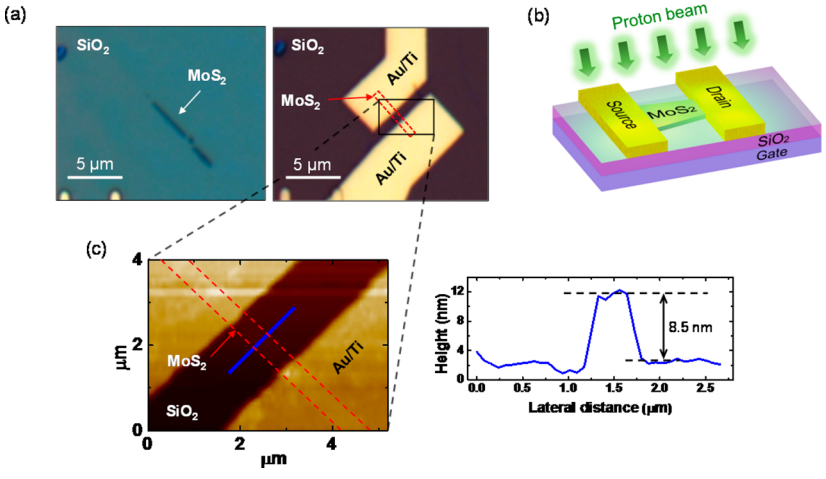

Figure 1. (a) Optical images showing the fabrication of a MoS_2 FET device. (b) Schematic illustration of proton beam irradiation on a MoS_2 FET device. (c) AFM image of the MoS_2 FET device with a cross-sectional topographic profile indicated by the blue line (MoS_2 flake). Red dashed lines in (a) and (c) indicate MoS_2 flakes.

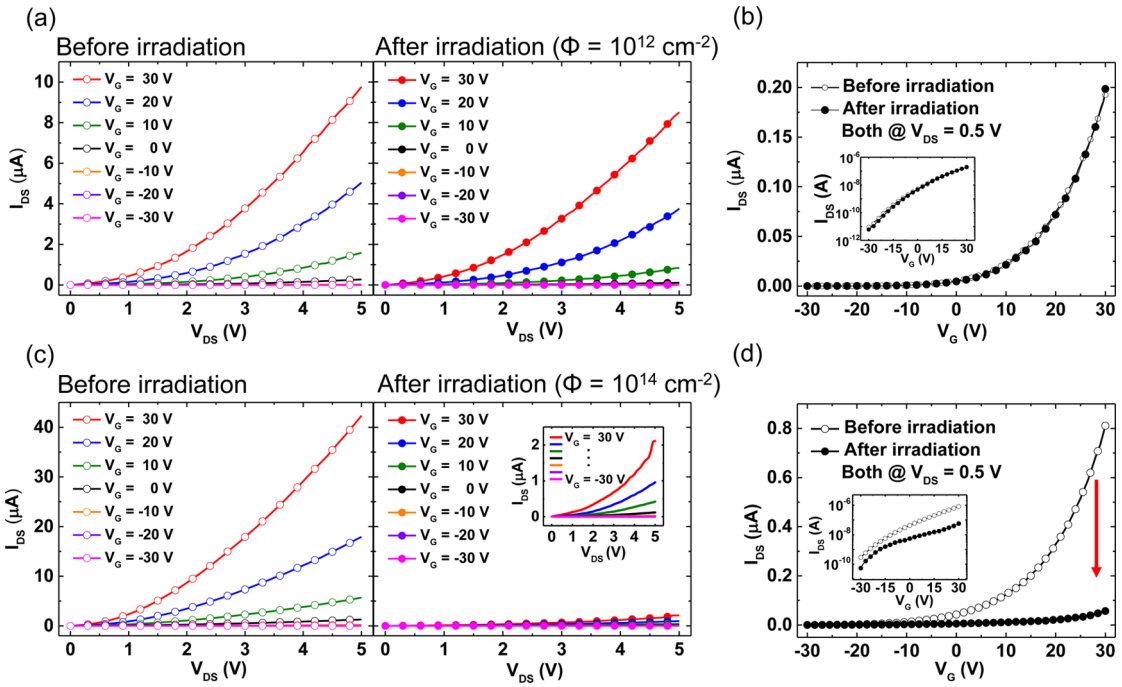

Figure 2. Representative electrical characteristics of MoS_2 FET devices. (a) Before and (b) after proton irradiation with a beam fluence of 10^{12} cm^{-2}. (c) Before and (d) after proton irradiation with a fluence of 10^{14} cm^{-2}. (a, c) Output characteristics ($I_{DS}-V_{DS}$) measured for different gate voltages. (b, d) Transfer characteristics ($I_{DS}-V_G$) measured at a fixed V_{DS} = 0.5 V. The inset figures of (b) and (d) are the transfer characteristics on a log scale.

shows the transfer characteristics (source−drain current *versus* gate voltage, $I_{DS}-V_G$) of the same device at a fixed source−drain voltage (V_{DS}) of 0.5 V before and after proton irradiation under the same proton beam conditions used in Figure 2a. The MoS_2 FET device exhibited n-channel behavior, with the current increasing as a more positive gate voltage was applied. The results in Figure 2a suggest that the electrical properties of the MoS_2 FET device did not change substantially following the proton irradiation with a small fluence condition of 10^{12} cm^{-2} (*i.e.*, a short proton irradiation time of 20 s). However, the MoS_2 FET devices were influenced noticeably when irradiated with the proton beam for a longer period of time. Figure 2c shows the output characteristics measured for another MoS_2 FET device before and after proton beam irradiation with a fluence of 10^{14} cm^{-2} (corresponding to an irradiation time of 2000 s). Figure 2d displays the corresponding transfer characteristics. Importantly, we observed that the current of the device decreased dramatically following proton beam irradiation. For example, the current of the device was measured as ~20 μA at V_{DS} = 5 V and V_G = 20 V prior to proton irradiation, whereas after proton irradiation, the current was measured as ~1 μA under the same measurement conditions (see inset of the plot on the right in Figure 2c). Hence, the current decreased by nearly 95% as a result of proton irradiation. This effect was clearly observed in the transfer curves (Figure 2d); that is, the current decreased significantly following proton beam irradiation. For the MoS_2 FET devices irradiated by a proton beam with a fluence of 10^{13} cm^{-2} (corresponding to an irradiation time of 200 s), the current level also decreased following proton irradiation, although the decrease was smaller than that observed under a fluence of 10^{14} cm^{-2}; the current decreased from ~17.5 μA (before proton irradiation) to ~5 μA (after proton irradiation) when measured at V_{DS} = 5 V and V_G = 20 V, as shown in Figure S2 of the Supporting Information. The subthreshold slope of the device that was irradiated with a low-fluence proton beam (10^{12} cm^{-2}) was almost the same before and after the proton irradiation, as shown in the inset of Figure 2b. On the contrary, the subthreshold slope of the device that was irradiated with a high-fluence proton beam (10^{14} cm^{-2}) became worse after the proton irradiation, as shown in the inset of Figure 2d. Such degradation of the subthreshold slope after high-fluence proton beam irradiation is attributed to the proton beam-induced trap states at the interface.

Figure 3a−c show the statistical results for the MoS_2 FET devices that were irradiated by proton beams under the three different fluence conditions. Here, we measured three devices under each fluence condition. A total of nine MoS_2 FET devices were therefore investigated, divided into three groups, and exposed to proton beams under the three different beam fluence conditions of 10^{12}, 10^{13}, and 10^{14} cm^{-2}. We subsequently compared the measurements before and after each proton irradiation condition. The error bars in the figures represent the standard deviations from the individual measurements. In Figure 3a, the current levels of the proton-irradiated devices

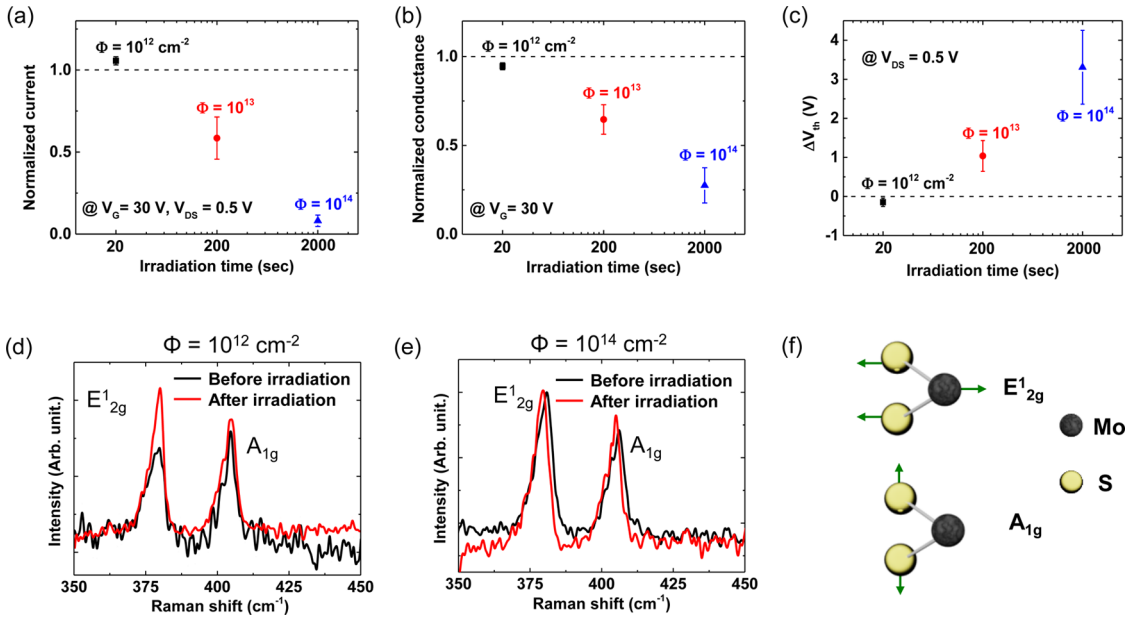

Figure 3. Statistical data for the (a) normalized conductance, (b) normalized current, and (c) change in the threshold voltage of the devices following proton irradiation with different beam fluences (10^{12}, 10^{13}, and 10^{14} cm^{-2}). Raman spectra of MoS_2 flakes before and after proton beam irradiation with the fluences of (d) $\Phi = 10^{12}$ cm^{-2} and (e) $\Phi = 10^{14}$ cm^{-2}. (f) Schematic illustrations of MoS_2 vibration modes.

measured at $V_G = 30$ V and $V_{DS} = 0.5$ V were compared with those of the devices before proton irradiation. The normalized current value in Figure 3a means the ratio of the current of the proton-irradiated device to that (value = 1.0, dashed line) of the same device before proton irradiation. In Figure 3b, the normalized conductance values were calculated and compared in a similar manner to that in Figure 3a. Here, the low-field conductance values were determined from the slope for a linear segment at the low bias region ($-0.3 < V_{DS} < 0.3$ V). Figure 3c displays the changes in threshold voltages following proton irradiation. First, the current, conductance, and threshold voltage values for the devices irradiated by proton beams under a low fluence of 10^{12} cm^{-2} did not change significantly. In contrast, for the devices irradiated by a proton beam with a medium fluence of 10^{13} cm^{-2}, the current and conductance values decreased substantially, accompanied with a shift of the threshold voltage to the positive gate voltage direction. These changes in the current, conductance, and threshold voltage became more significant for the devices irradiated by proton beams with a high fluence of 10^{14} cm^{-2}, as indicated by the greater decreases in the current and conductance and the more positive shifts of the threshold voltage.

We measured Raman spectra of MoS_2 flakes before and after proton beam irradiation with fluences of $\Phi = 10^{12}$ cm^{-2} (Figure 3d) and $\Phi = 10^{14}$ cm^{-2} (Figure 3e). The two prominent E^1_{2g} (~380 cm^{-1}) and A_{1g} (~405 cm^{-1}) peaks are due to in-plane and out-of-plane vibrations of MoS_2 atoms,[28] as illustrated in Figure 3f. There was no significant change found in the E^1_{2g} and A_{1g} modes of MoS_2 in the Raman spectra before and after the proton irradiation. Note that we did Raman or electrical measurements on the proton-irradiated samples at least 1 day after the proton irradiation because we were not allowed to pick up the proton-exposed samples right after the proton irradiation due to radioactivity safety regulations. Importantly, we observed significant changes in the electrical properties of MoS_2 FETs (Figures 2 and 3a–c), while we did not observe noticeable changes in the Raman spectra of MoS_2 flakes (Figures 3d,e). These results suggest that the change of the electrical characteristics of MoS_2 FET devices after the proton irradiation is not due to MoS_2 itself; instead it is due to the proton-irradiation-induced oxide traps in the SiO_2 layer or the interface trap states at the SiO_2/MoS_2 interface.

We investigated the time-dependence of the electrical characteristics of the proton-irradiated devices by measuring the devices before proton irradiation and 1 day, 3 days, and 5 days after proton irradiation. Figure 4a–c show the transfer curves of three MoS_2 FET devices that were irradiated by proton beams with fluence conditions of either 10^{12}, 10^{13}, or 10^{14} cm^{-2}. For the 10^{12} cm^{-2} fluence condition, the current of the proton-irradiated device remained nearly constant with time (Figure 4a), consistent with the results of Figures 2 and 3. For the cases of the 10^{13} and 10^{14} cm^{-2} fluences, the currents of the proton-irradiated devices decreased following proton irradiation (for example, see the day 1 data). However, the current typically recovered; for the middle fluence condition (10^{13} cm^{-2}), the current recovered to nearly its original level after 5 days (Figure 4b), whereas for the high-fluence condition (10^{14} cm^{-2}), the current recovered

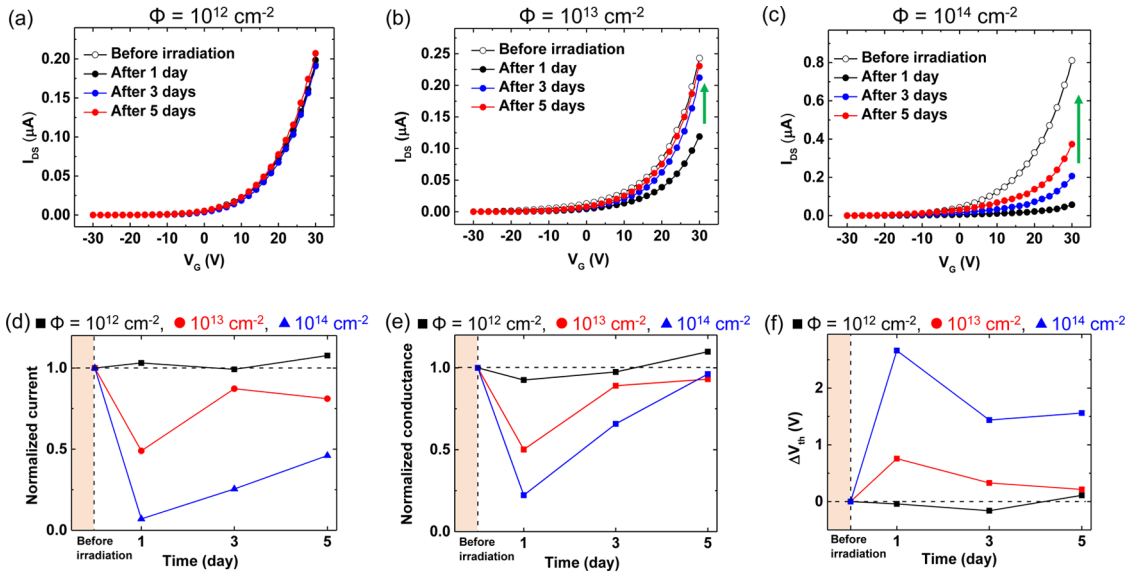

Figure 4. Time-dependence of the $I_{DS}-V_G$ curves of the MoS_2 FET devices before proton irradiation and 1, 3, and 5 days after proton irradiation with fluences of (a) 10^{12} cm^{-2}, (b) 10^{13} cm^{-2}, and (c) 10^{14} cm^{-2}. The (d) normalized current, (e) normalized conductance, and (f) change in the threshold voltages of the devices are plotted as a function of time (*i.e.*, before proton irradiation and at 1, 3, and 5 days after proton irradiation) for the three different fluence conditions of 10^{12}, 10^{13}, and 10^{14} cm^{-2}.

but remained diminished even after 5 days (Figure 4c). Figure 4d–f summarize the normalized current, normalized conductance, and changes in the threshold voltage before and after proton irradiation with fluence conditions of 10^{12}, 10^{13}, and 10^{14} cm^{-2}. These plots show that the electrical parameters were not significantly influenced by the weak fluence proton irradiation (10^{12} cm^{-2}) and that these values typically recovered with time but that the recovery was not complete for the high-fluence proton irradiation (10^{14} cm^{-2}).

We now discuss the results of our proton irradiation experiments on MoS_2 FET devices. When high-energy particles are irradiated on silicon-based materials and devices, they lose the majority of their energy near the stopping position.[29,30] We calculated the energy-loss depth profiles of irradiated protons using Stopping and Range of Ions in Matter (SRIM 2008) software, which is a computer program that calculates the interactions of energetic particles with matter. The SRIM simulation results are provided in Figure S5 of the Supporting Information.[30,31] From these simulation results, we found that protons could penetrate and stop ~700 μm from the top surface. Because the structure of our MoS_2 FET devices comprised stacks of $MoS_2/SiO_2/Si$ (2–8 nm/270 nm/500 μm), the majority of protons could simply penetrate through the entire structure, generating electron–hole pairs along the path of the proton beam. It is known that when high-energy particles such as electrons and protons are irradiated on silicon-based FET devices, they can ionize atoms and generate electron–hole pairs in the oxide (SiO_2) layer, which is the layer that is most sensitive to ionizing irradiation.[32,33] The generated electrons are quickly swept out of the bulk SiO_2 layer in a few picoseconds due to their high mobility.[34] The remaining holes wander through the SiO_2 layer and may be trapped at localized trap sites in the bulk SiO_2 layer, leading to positive oxide-trapped charges. In addition, the irradiation-induced holes and protons in the SiO_2 can transport to the SiO_2/MoS_2 interface, leading to the formation of interface trap states, which are negatively charged electron trap centers for n-channel transistors. The positive oxide traps in the SiO_2 layer enhance the gate electric field, leading to an increased carrier concentration. In contrast, the negative interface trap states act as electron trap centers, leading to a reduction in the carrier concentration. Furthermore, the irradiation-induced interface trap states occur on a time scale that is much slower than that of the positive oxide-charge traps in the SiO_2 layer. Therefore, the effects of proton irradiation on the MoS_2 FET devices can be attributed to the combined effects of positive oxide-charge traps in the SiO_2 layer and interface trap states.[35–37]

For low-fluence (short irradiation time) proton irradiation, neither positive oxide-charge traps nor interface trap states will be generated in sufficient quantities to significantly affect the electrical characteristics of the devices. As a result, no significant changes in the electrical parameters of the proton-irradiated devices were observed for proton irradiation under a 10^{12} cm^{-2} fluence (see Figures 2a,b, 3a–c, 4a and d–f). However, at high fluence (long irradiation time), the interface trap states will play a major role in influencing the electrical performances of the proton-irradiated devices. These effects were observed in the MoS_2 FET devices irradiated by proton beams with 10^{13} or 10^{14} cm^{-2} fluences (Figures 2c,d, 3a–c, and 4b–f). Note that for the 10^{12} cm^{-2} fluence condition, the currents of a portion of the proton-irradiated devices increased slightly

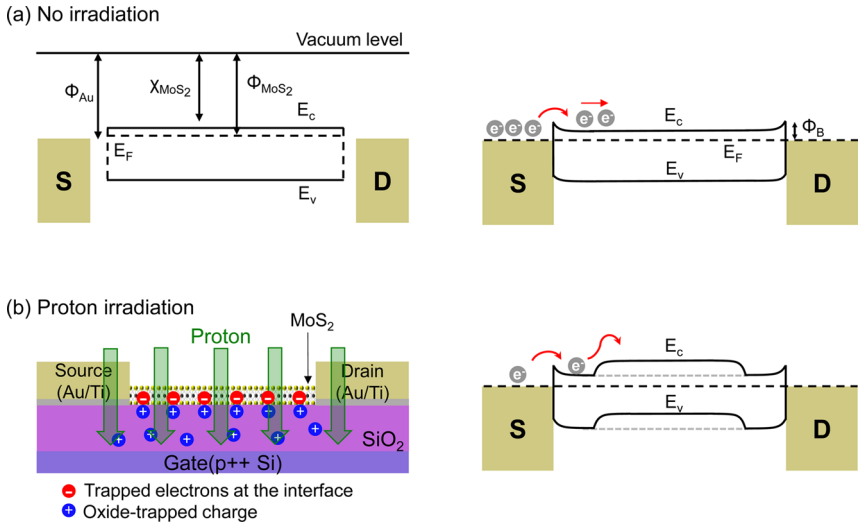

Figure 5. Energy band diagrams of a MoS_2 FET device (a) prior to proton irradiation (no irradiation) and (b) after proton irradiation with high beam fluence (10^{13} and 10^{14} cm^{-2}). E_F: Fermi level energy, E_C: conduction band minimum, E_V: valence band maximum, Φ_B: Schottky barrier height. The green arrow indicates the proton beam irradiation, the blue circles with plus signs represent the oxide-trapped charges, and the red circles with minus signs represent the interface-trapped charges.

compared with those measured prior to proton irradiation (see Figure 3a), which could be due to the effect of positive oxide-trap charges in the SiO_2 layer. However, this effect was too small to be confirmed, and a modified experimental design would be necessary to distinguish the effect of the positive oxide-trap charges in the SiO_2 layer from that of the interface trap states. The recovery phenomena (Figure 4) can also be attributed to the traps generated by the proton irradiation.[37,38] The recovery of the current indicates that the proton-irradiation-induced traps are not permanent and do not act as charge traps for an extended period unless the fluence of the proton irradiation is beyond a certain threshold. We observed that the current was fully recovered for a middle fluence of 10^{13} cm^{-2} approximately 5 days after proton irradiation (Figure 4b), but was not fully recovered at this time point for the high fluence condition of 10^{14} cm^{-2} (Figure 4c).

The observations in this study can be explained using energy band diagrams, as shown in Figure 5. Figure 5a shows the energy band diagrams for V_{DS} = 0 V and V_G = 0 V. The MoS_2 flakes have a band gap of ~1.2 eV, which is similar to the band gap of bulk MoS_2.[8] In addition, the work function (Φ_{MoS2}) and electron affinity (χ_{MoS2}) of the flakes are 4.6−4.9 eV and ~4.0 eV, respectively.[39−42] We used Au/Ti as the source and drain electrodes in contact with the MoS_2 and a work function for Au (Φ_{Au}) of 5.4 eV and that for Ti (Φ_{Ti}) of 4.3 eV.[41] Therefore, the contact between Ti and MoS_2 will have a very small Schottky barrier (Φ_B), as indicated in the energy band diagram (Figure 5a, right).[41] When protons are irradiated on the devices, the proton beam induces positive oxide-trap charges in the SiO_2 layer and interface trap states at the SiO_2/MoS_2 interface. When the proton beam fluence is sufficient, the interface trap states influence the current flow in the MoS_2 channel, which hinders charge flows by trapping conduction electrons in the n-channel MoS_2. This will decrease the conduction electron concentration, raising the conduction band. In other words, an increasing interface trap density in the channel region by proton irradiation increases trapped electrons in the channel and reduces the current conductance, as shown in the right panel in Figure 5b.

CONCLUSION

In summary, we studied the effect of proton beam irradiation on multilayer MoS_2 FET devices. The n-channel MoS_2 FET devices irradiated by proton beams with sufficiently high fluence conditions exhibited decreases in the current and conductance and a shift of the threshold voltage toward the positive gate voltage direction. The recovery of these changes was observed over a time scale of days. These phenomena can be attributed to the interface trap states at the SiO_2/MoS_2 interfaces. This study improves our understanding of the influence of high-energy proton beams on MoS_2-based nanoelectronic devices and may provide a method to control the electrical properties of MoS_2 FET devices through changing interface states using proton beams.

METHODS

The multilayer MoS_2 was exfoliated using the micromechanical exfoliation method from a bulk MoS_2 crystal purchased from SPI Supplier. The multilayer MoS_2 flakes were transferred by 3M Scotch tape to SiO_2 on a heavily doped p++ Si wafer (resistivity ~5 × 10^{-3} Ω cm) that can be used as a back gate.

The location of a MoS_2 flake was found using an optical microscope; then the MoS_2 flake's height was measured with an NX 10 AFM system (Park Systems). In order to make patterns of electrodes, we spin-coated MMA (8.5), MAA (9% concentration in ethyl lactate), and PMMA 950K (5% concentration in anisole) at 4000 rpm. After the two-step spin-coating, the sample was baked at 180 °C for 90 s on a hot plate. The electrodes were patterned using an electron beam lithography system (JSM-6510, JEOL) with a 30 kV exposure. For the development of pattern, MIBK/IPA (1:3) solution was used with a development time of 50 s. All the electrical measurements were conducted with a probe station (JANIS, ST-500) using a semiconductor parameter analyzer (HP 4145B) at room temperature in a vacuum ($\sim 10^{-4}$ Torr).

The Raman spectroscopic measurements were done with a Raman spectrometer (T64000 Horiba Jobin Yvon, at National Center for Inter-University Research Facilities) that uses an Ar ion laser (wavelength of 514.5 nm) as a source.

Conflict of Interest: The authors declare no competing financial interest.

Supporting Information Available: MoS_2 FET device fabrication procedures, output and transfer characteristics of a device that was irradiated by a proton beam with a fluence of 10^{13} cm^{-2}, Raman spectroscopy data for the MoS_2 flakes before and after proton irradiation with fluence conditions of 10^{12} and 10^{14} cm^{-2}, and SRIM simulation data. This material is available free of charge *via* the Internet at http://pubs.acs.org.

Acknowledgment. The authors appreciate the financial support of the National Creative Research Laboratory program (Grant No. 2012026372) and the National Core Research Center program (Grant No. 2008-0062606) through the National Research Foundation of Korea (NRF) funded by the Korean Ministry of Science, ICT & Future Planning. We are especially thankful for the beam time grants from the proton beam facilities of the Korea Institute of Radiological and Medical Sciences, and the Korea Multi-Purpose Accelerator Complex (KOMAC) of Korea Atomic Energy Research Institute (KAERI). S.H. acknowledges the support from the NRF grant (H-GUARD 2013M3A6B2078961).

REFERENCES AND NOTES

1. Chhowalla, M.; Shin, H. S.; Eda, G.; Li, L.-J.; Loh, K. P.; Zhang, H. The Chemistry of Two-Dimensional Layered Transition Metal Dichalcogenide Nanosheets. *Nat. Chem.* **2013**, *5*, 263–275.
2. Wang, Q. H.; Kalantar-Zadeh, K.; Kis, A.; Coleman, J. N.; Strano, M. S. Electronics and Optoelectronics of Two-Dimensional Transition Metal Dichalcogenides. *Nat. Nanotechnol.* **2012**, *7*, 699–712.
3. Fang, H.; Chuang, S.; Chang, T. C.; Takei, K.; Takahashi, T.; Javey, A. High-Performance Single Layered WSe_2 p-FETs with Chemically Doped Contacts. *Nano Lett.* **2012**, *12*, 3788–3792.
4. Mak, K. F.; Lee, C.; Hone, J.; Shan, J.; Heinz, T. F. Atomically Thin MoS_2: A New Direct-Gap Semiconductor. *Phys. Rev. Lett.* **2010**, *105*, 136805.
5. Schwierz, F. Graphene Transistors. *Nat. Nanotechnol.* **2010**, *5*, 487–496.
6. Jiang, H. Electronic Band Structures of Molybdenum and Tungsten Dichalcogenides by the GW Approach. *J. Phys. Chem. C* **2012**, *116*, 7664–7671.
7. Coehoorn, R.; Haas, C.; Dijkstra, J.; Flipse, C.; De Groot, R.; Wold, A. Electronic Structure of $MoSe_2$, MoS_2, and WSe_2. I. Band-Structure Calculations and Photoelectron Spectroscopy. *Phys. Rev. B* **1987**, *35*, 6195.
8. Kam, K.; Parkinson, B. Detailed Photocurrent Spectroscopy of the Semiconducting Group VI Transition Metal Dichalcogenides. *J. Phys. Chem.* **1982**, *86*, 463–467.
9. Yoon, J.; Park, W.; Bae, G. Y.; Kim, Y.; Jang, H. S.; Hyun, Y.; Lim, S. K.; Kahng, Y. H.; Hong, W. K.; Lee, B. H. Highly Flexible and Transparent Multilayer MoS_2 Transistors with Graphene Electrodes. *Small* **2013**, *9*, 3295–3300.
10. Sundaram, R. S.; Engel, M.; Lombardo, A.; Krupke, R.; Ferrari, A. C.; Avouris, P.; Steiner, M. Electroluminescence in Single Layer MoS_2. *Nano Lett.* **2013**, *13*, 1416–1421.
11. Radisavljevic, B.; Kis, A. Mobility Engineering and a Metal-Insulator Transition in Monolayer MoS_2. *Nat. Mater.* **2013**, *12*, 815–820.
12. Lopez-Sanchez, O.; Lembke, D.; Kayci, M.; Radenovic, A.; Kis, A. Ultrasensitive Photodetectors based on Monolayer MoS_2. *Nat. Nanotechnol.* **2013**, *8*, 497–501.
13. Lee, H. S.; Min, S.-W.; Chang, Y.-G.; Park, M. K.; Nam, T.; Kim, H.; Kim, J. H.; Ryu, S.; Im, S. MoS_2 Nanosheet Phototransistors with Thickness-Modulated Optical Energy Gap. *Nano Lett.* **2012**, *12*, 3695–3700.
14. Kim, S.; Konar, A.; Hwang, W.-S.; Lee, J. H.; Lee, J.; Yang, J.; Jung, C.; Kim, H.; Yoo, J.-B.; Choi, J.-Y. High-Mobility and Low-Power Thin-Film Transistors based on Multilayer MoS_2 Crystals. *Nat. Commun.* **2012**, *3*, 1011.
15. Radisavljevic, B.; Radenovic, A.; Brivio, J.; Giacometti, V.; Kis, A. Single-Layer MoS_2 Transistors. *Nat. Nanotechnol.* **2011**, *6*, 147–150.
16. Vijayaraghavan, A.; Kanzaki, K.; Suzuki, S.; Kobayashi, Y.; Inokawa, H.; Ono, Y.; Kar, S.; Ajayan, P. M. Metal-Semiconductor Transition in Single-Walled Carbon Nanotubes Induced by Low-Energy Electron Irradiation. *Nano Lett.* **2005**, *5*, 1575–1579.
17. Gomez-Navarro, C.; De Pablo, P.; Gómez-Herrero, J.; Biel, B.; Garcia-Vidal, F.; Rubio, A.; Flores, F. Tuning the Conductance of Single-Walled Carbon Nanotubes by Ion Irradiation in the Anderson Localization Regime. *Nat. Mater.* **2005**, *4*, 534–539.
18. Gunho, J.; Hong, W.-K.; Choe, M.; Park, W.; Yung, H. K.; Lee, T. Proton Irradiation-Induced Electrostatic Modulation in ZnO Nanowire Field-Effect Transistors with Bilayer Gate Dielectric. *IEEE Trans. Nanotechnol.* **2012**, *11*, 918–923.
19. Hong, W.-K.; Jo, G.; Sohn, J. I.; Park, W.; Choe, M.; Wang, G.; Kahng, Y. H.; Welland, M. E.; Lee, T. Tuning of the Electronic Characteristics of ZnO Nanowire Field Effect Transistors by Proton Irradiation. *ACS Nano* **2010**, *4*, 811–818.
20. Liao, L.; Lu, H.; Li, J.; Liu, C.; Fu, D.; Liu, Y. The Sensitivity of Gas Sensor Based on Single ZnO Nanowire Modulated by Helium Ion Radiation. *Appl. Phys. Lett.* **2007**, *91*, 173110.
21. Childres, I.; Jauregui, L. A.; Foxe, M.; Tian, J.; Jalilian, R.; Jovanovic, I.; Chen, Y. P. Effect of Electron-Beam Irradiation on Graphene Field Effect Devices. *Appl. Phys. Lett.* **2010**, *97*, 173109.
22. Hu, X.; Karmarkar, A. P.; Jun, B.; Fleetwood, D. M.; Schrimpf, R. D.; Geil, R. D.; Weller, R. A.; White, B. D.; Bataiev, M.; Brillson, L. J. Proton-Irradiation Effects on AlGaN/AlN/GaN High Electron Mobility Transistors. *IEEE Trans. Nucl. Sci.* **2003**, *50*, 1791–1796.
23. Krasheninnikov, A.; Nordlund, K.; Sirviö, M.; Salonen, E.; Keinonen, J. Formation of Ion-Irradiation-Induced Atomic-Scale Defects on Walls of Carbon Nanotubes. *Phys. Rev. B* **2001**, *63*, 245405.
24. Srour, J. R.; McGarrity, J. M. Radiation Effects on Microelectronics in Space. *Proc. IEEE* **1988**, *76*, 1443–1469.
25. Komsa, H.-P.; Kotakoski, J.; Kurasch, S.; Lehtinen, O.; Kaiser, U.; Krasheninnikov, A. V. Two-Dimensional Transition Metal Dichalcogenides under Electron Irradiation: Defect Production and Doping. *Phys. Rev. Lett.* **2012**, *109*, 035503.
26. Ochedowski, O.; Marinov, K.; Wilbs, G.; Keller, G.; Scheuschner, N.; Severin, D.; Bender, M.; Maultzsch, J.; Tegude, F. J.; Schleberger, M. Radiation Hardness of Graphene and MoS_2 Field Effect Devices against Swift Heavy Ion Irradiation. *J. Appl. Phys.* **2013**, *113*, 214306.
27. Mathew, S.; Gopinadhan, K.; Chan, T.; Yu, X.; Zhan, D.; Cao, L.; Rusydi, A.; Breese, M.; Dhar, S.; Shen, Z. Magnetism in MoS_2 Induced by Proton Irradiation. *Appl. Phys. Lett.* **2012**, *101*, 102103.
28. Lee, C.; Yan, H.; Brus, L. E.; Heinz, T. F.; Hone, J.; Ryu, S. Anomalous Lattice Vibrations of Single-and Few-Layer MoS_2. *ACS Nano* **2010**, *4*, 2695–2700.
29. Messenger, S.; Burke, E.; Summers, G.; Xapsos, M.; Walters, R.; Jackson, E.; Weaver, B. Nonionizing Energy Loss (NIEL) for Heavy Ions. *IEEE Trans. Nucl. Sci.* **1999**, *46*, 1595–1602.

30. Ziegler, J. F.; Biersack, J. P. *The Stopping and Range of Ions in Matter*; Springer: Berlin, 1985.
31. Ziegler, J. F.; Ziegler, M. D.; Biersack, J. P. SRIM-The Stopping and Range of Ions in Matter. *Nucl. Instrum. Methods Phys. Res., Sect. B* **2010**, *268*, 1818–1823.
32. Schroder, D. K. *Semiconductor Material and Device Characterization*; John Wiley & Sons: New York, 2006; Chapter 6.
33. Oldham, T. R. *Ionizing Radiation Effects in MOS Oxides*; World Scientific: Singpore, 1999; Vol. 3.
34. Hughes, R. Chrage-Carrier Transport Phenomena in Amorphous SiO_2: Direct Measurement of the Drift Mobility and Lifetime. *Phys. Rev. Lett.* **1973**, *30*, 1333.
35. Sze, S. M.; Ng, K. K. *Physics of Semiconductor Devices*, 3rd ed.; Wiley-Interscience: New York, 2007; Chapter 4.
36. Schwank, J. R.; Shaneyfelt, M. R.; Fleetwood, D. M.; Felix, J. A.; Dodd, P. E.; Paillet, P.; Ferlet-Cavrois, V. Radiation Effects in MOS Oxides. *IEEE Trans. Nucl. Sci.* **2008**, *55*, 1833–1853.
37. Oldham, T. R.; McLean, F. Total Ionizing Dose Effects in MOS Oxides and Devices. *IEEE Trans. Nucl. Sci.* **2003**, *50*, 483–499.
38. McLean, F.; Boesch, H.; McGarrity, J. Hole Transport and Recovery Characteristics of SiO_2 Gate Insulators. *IEEE Trans. Nucl. Sci.* **1976**, *23*, 1506–1512.
39. Liu, K.-K.; Zhang, W.; Lee, Y.-H.; Lin, Y.-C.; Chang, M.-T.; Su, C.-Y.; Chang, C.-S.; Li, H.; Shi, Y.; Zhang, H. Growth of Large-Area and Highly Crystalline MoS_2 Thin Layers on Insulating Substrates. *Nano Lett.* **2012**, *12*, 1538–1544.
40. Giridharagopal, R.; Kelly, K. F. Substrate-Dependent Properties of Polydiacetylene Nanowires on Graphite and MoS_2. *ACS Nano* **2008**, *2*, 1571–1580.
41. Das, S.; Chen, H.-Y.; Penumatcha, A. V.; Appenzeller, J. High Performance Multilayer MoS_2 Transistors with Scandium Contacts. *Nano Lett.* **2013**, *13*, 100–105.
42. Han, S.; Kwon, H.; Kim, S. K.; Ryu, S.; Yun, W. S.; Kim, D.; Hwang, J.; Kang, J.-S.; Baik, J.; Shin, H. Band-Gap Transition Induced by Interlayer Van Der Waals Interaction in MoS_2. *Phys. Rev. B* **2011**, *84*, 045409.